IOP Publishing Journal of Physics D: Applied Physics
J. Phys. D: Appl. Phys. **53** (2020) 355301 (11pp) https://doi.org/10.1088/1361-6463/ab8fe0

Contact resistance and current crowding in tunneling type circular nano-contacts

Sneha Banerjee, Patrick Y Wong and Peng Zhang

Department of Electrical and Computer Engineering, Michigan State University, East Lansing, MI 48824-1226, United States of America

E-mail: pz@egr.msu.edu

Received 5 February 2020, revised 28 April 2020
Accepted for publication 4 May 2020
Published 17 June 2020

Abstract

Current transport and contact resistance in nanoscale electrical contacts are important to the overall device properties, especially for devices based on novel one-dimensional and two-dimensional materials or nanostructures. In this paper, we present a self-consistent method to model tunneling type circular thin film contacts. We solve the lumped circuit circular transmission line model (CTLM) with tunneling-induced specific contact resistivity ρ_c which varies along the radial direction. The contacting members are separated by a thin insulating layer, where the radially dependent ρ_c is calculated from local voltage dependent tunneling current density. The current and voltage distributions in such contacts and their overall contact resistance are studied in detail, for various input voltages, contact dimensions, and material properties (i.e. work function, sheet resistance of the contact members, and permittivity of the insulating layer). Our study shows that the contact resistance is voltage dependent, and the radial current distribution is strongly nonhomogeneous. The contact resistance and the current distribution can be controlled by engineering the contact layer properties and geometry radially. Although focused on Schrödinger tunneling type contacts in this work, our modified CTLM equations with radially varying ρ_c are general, and may be readily used for other types of electrical contacts, such as ohmic and Schottky contacts.

Keywords: contact resistance, current crowding, quantum tunneling, circular electrical contact

(Some figures may appear in colour only in the online journal)

1. Introduction

Current transport and contact resistance in nanoscale electrical contacts are recently being studied extensively to meet the growing demands for the physical shrinking of electronic circuits [1]. Advancements in the development of novel one-dimensional (1D) and two-dimensional (2D) materials and nanostructure-based devices have also contributed to the growing research interest in electrical contacts [2–4]. Although popular for their unique electrical and mechanical properties, the nanowire, nanotube, nanorod, and nanofiber-based devices face serious challenges because of a large number of electrical contacts usually present in the circuit. Electrical properties in these nano contacts impact the controllability, reliability, and efficiency of the overall device [5, 6]. Moreover, contact resistance in electronic devices composed of a single layer or multilayer 2D material based thin films (e.g. graphene, boron nitride, molybdenum sulfide, black phosphorus, tungsten disulfide, etc), restricts their large-scale industrial production [7]. Hence, controlling current transport in nano-contacts is a fundamental step towards many technological breakthroughs.

For decades, the transmission line model (TLM) has been widely used with great success to analyze electrical properties in nano-scale and meso-scale contacts [8–14]. Recently Banerjee *et al* [15] modified the conventional TLM for parallel Cartesian nanocontacts including the effects of spatially varying specific contact resistivity ρ_c. In this paper, we extend that work to demonstrate a 2D circular transmission line model (CTLM) for circular and annular nanocontacts. Circular tunneling contacts may be formed between two thin films or between a thin film substrate and a standing cylindrical nanorod (or nanofiber) as in the configuration of field emitters [16, 17]. Like [15], our model is two-dimensional in the sense

that we consider radial variation in the contact resistivity ρ_c, which may be introduced by a variety of factors. For instance, the inherent non-linearity of the current density-voltage ($J-V$) profiles of tunneling [18, 19] and Schottky junctions [20] may lead to strong radial dependence of the electrical properties in practical 2D contacts. Radial variation of the interfacial layer thickness for tunneling type contacts and nonuniform distribution of contaminants or impurities in the contact layer for ohmic or Schottky contacts can also cause radially changing ρ_c. Our model can be applied to characterize electrical properties in nanoscale thin film contacts, circular gate transistors (CGTs) [21], nanorod [22], nanowire [23], nano-fiber [16], and novel 2D material based devices [24].

The tunneling type of nanocontacts, where a thin (in nanometer or sub-nanometer range) interfacial layer (vacuum or insulator) exists between the two contact members [15, 25, 26], are ubiquitous. The local tunneling dependent ρ_c was calculated from the Simmons formula [27, 28] in Banerjee *et al* [15]. Although the Simmons tunneling current formulas [27, 28] reveal basic scaling and parametric dependence of the $J-V$ profiles in metal-insulator-metal (MIM) nanogaps for low voltages, they ignore the effects of exchange correlation potential and the space charge potential inside the gap, which can modify the tunneling current density by several orders of magnitude [18, 19]. Here we incorporate a more accurate quantum analysis based on the self-consistent Schrödinger-Poisson solutions [18, 19], into the 2D circular TLM to calculate the local voltage dependent tunneling resistivity along the radial contact length. We find that the contact resistance is voltage dependent, and for intermediate voltages when the tunneling junction is operated in the field emission regime [18, 19], the dependence is the strongest. We also find that the radial current distribution is highly nonhomogeneous. This non-homogeneity can be manipulated by engineering the contact layer properties and geometry radially.

In section 2, the formulation of our 2D CTLM is presented. Results and discussions are presented in section 3, where we consider two cases. Firstly, we assume constant specific contact resistivity along the radial contact length and obtain analytical expressions for the local voltage, current, and total contact resistance. Secondly, we perform numerical calculations for nanocontacts with spatially dependent contact resistivity induced by local quantum tunneling phenomenon [18, 19]. Summary and suggestions for future research are given in section 4. Although we focus on tunneling type electrical contacts here, the proposed 2D CTLM is general and can be used for other types of circular and annular electrical contacts, such as nanoscale ohmic contacts and Schottky contacts based on 2D materials heterostructure [3, 20, 29, 30].

2. Formulation

Consider a circular (ring) contact formed between two conducting thin films or layers, as shown in figures 1(a) and (b). The outer radius of thin film 2 is r_o and the inner radius of both the films is r_i. A thin resistive interface layer of thickness D is sandwiched between them. Following Reeves [11–13], we modified the basic Cartesian geometry lumped circuit transmission line model (TLM) [8, 9, 14, 31] for circular structures, as shown in figure 1(c). The sheet resistance of the two conductors is R_{sh1} and R_{sh2}, respectively. The radially dependent specific interfacial resistivity (also termed specific contact resistivity) is $\rho_c(r)$, which is either predefined or calculated from the local tunneling current in the case of an insulating tunneling layer [18, 19, 27, 28, 32].

In the contact region in figure 1(c), when $\Delta r \to 0$, Kirchhoff's laws for current and voltage give the following equations,

$$\frac{dI_1(r)}{dr} = 2\pi r\, J_c(r)\,, \tag{1a}$$

$$\frac{dV_1(r)}{dr} = \frac{I_1(r)\,R_{sh1}}{2\pi r}, \tag{1b}$$

$$\frac{dI_2(r)}{dr} = -\,2\pi r\, J_c(r)\,, \tag{1c}$$

$$\frac{dV_2(r)}{dr} = \frac{I_2(r)\,R_{sh2}}{2\pi r}, \tag{1d}$$

where $I_1(r)$ and $I_2(r)$ represent the currents flowing at r along the radial direction of thin films 1 and 2, respectively, and $V_1(r)$ and $V_2(r)$ are the local voltages at r along the radial direction of thin films 1 and 2, respectively. $J_c(r) = V_g(r)/\rho_c(r)$ and $V_g(r) = V_1(r) - V_2(r)$ are the local current density and the local voltage drop across the contact interface at r, respectively.

From equations 1(a) and 1(c), $I_1(r) + I_2(r) = I_{tot} =$ constant, where I_{tot} is the total current in the circuit to be determined from the following boundary conditions for equation (1),

$$\begin{aligned} &V_1(r = r_o) = V_o, I_1(r = r_i) = 0, I_2(r = r_o) = 0, \\ &V_2(r = r_i) = 0, \end{aligned} \tag{2}$$

where we assume the voltage of the upper contact member at $r = r_i$ is 0 and the external voltage V_0 is applied at $r = r_o$ to the lower contact member. Note that $I_1(r = r_o) = I_{tot}$, $I_2(r = r_i) = I_{tot}$, and $I_{tot} = \int_{r_i}^{r_o} 2\pi r\, J_c(r)\; dr$. From equations (1) and (2), we get $V_1'(r = r_o) = I_{tot}R_{sh1}/2\pi r_o$, $V_1'(r = r_i) = 0$, $V_2'(r = r_o) = 0$, $V_2'(r = r_i) = I_{tot}R_{sh2}/2\pi r_i$, where a prime denotes a derivative with respect to r. For the contact model in figure 1(c), the contact resistance is defined as,

$$R_c = \frac{V_1(r_o) - V_2(r_i)}{I_{tot}} = \frac{V_o}{I_{tot}}. \tag{3}$$

For convenience, we introduce non-dimensional quantities, $\bar{r} = r/r_o$, $\beta = r_i/r_o$, $\bar{\rho}_c(\bar{r}) = \rho_c(r)/(R_{sh1}r_o^2)$, $\overline{R_{sh2}} = R_{sh2}/R_{sh1}$, $\overline{J_c}(\bar{r}) = J_c(r)R_{sh1}r_o^2/V_o$, $\overline{V_1}(\bar{r}) = V_1(r)/V_o$, $\overline{V_2}(\bar{r}) = V_2(r)/V_o$, $\overline{V_g}(\bar{r}) = V_g(r)/V_o$, $\overline{R_c} = R_c 2\pi/R_{sh1}$, and $\alpha = I_{tot}/I$, where $I = 2\pi V_o/R_{sh1}$. In normalized forms,

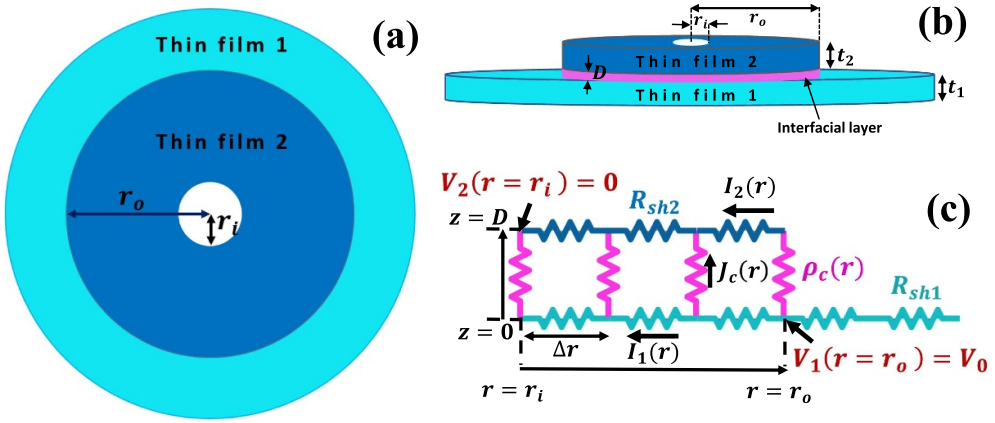

Figure 1. Electrical contact between two circular thin films: (a) top view; (b) side view; (c) its transmission line model. (a)–(c) A thin resistive interface layer (or a tunneling layer of permittivity ε_r) of thickness D is sandwiched between the two contacting members. The thicknesses of thin film 1 and 2 are t_1 and t_2, respectively.

equation (1) can be written into the following coupled second order differential equations,

$$\frac{d^2\overline{V_1}(\bar{r})}{d\bar{r}^2} + \frac{1}{\bar{r}}\frac{d\overline{V_1}(\bar{r})}{d\bar{r}} - \frac{\overline{V_1}(\bar{r}) - \overline{V_2}(\bar{r})}{\overline{\rho_c}(\bar{r})} = 0, \tag{4a}$$

$$\frac{d^2\overline{V_2}(\bar{r})}{d\bar{r}^2} + \frac{1}{\bar{r}}\frac{d\overline{V_2}(\bar{r})}{d\bar{r}} + \overline{R_{sh2}}\frac{\overline{V_1}(\bar{r}) - \overline{V_2}(\bar{r})}{\overline{\rho_c}(\bar{r})} = 0. \tag{4b}$$

Note that $\overline{V_g}(\bar{r}) = \overline{V_1}(\bar{r}) - \overline{V_2}(\bar{r})$ and $\overline{J_c}(\bar{r}) = \overline{V_g}(\bar{r})/\overline{\rho_c}(\bar{r})$. The corresponding boundary conditions to equation (4) are,

$$\overline{V_1}(\bar{r} = 1) = 1,\ \overline{V_1}'(\bar{r} = 1) = \alpha,\ \overline{V_1}'(\bar{r} = \beta) = 0, \tag{5a}$$

$$\overline{V_2}(\bar{r} = \beta) = 0,\ \overline{V_2}'(\bar{r} = 1) = 0,\ \overline{V_2}'(\bar{r} = \beta) = \frac{\alpha\overline{R_{sh2}}}{\beta}, \tag{5b}$$

and the normalized total current,

$$\alpha = I_{tot}/I = \int_{\beta}^{1} \bar{r}\,\overline{J_c}(\bar{r})\,d\bar{r}. \tag{5c}$$

Equations (4) and (5) are solved to give the voltage distribution along and across the contact interface as well as the total contact resistance, for a given electrical contact (figure 1) with radially dependent interface specific contact resistivity $\overline{\rho_c}(\bar{r})$, following a similar procedure as described in [15]. Equations (4) and (5) can be solved numerically for arbitrary radial dependence of specific contact resistivity $\overline{\rho_c}(\bar{r})$. Here, we focus on two special cases of practical importance. We first consider the case of constant $\overline{\rho_c}$, where analytical solutions can be obtained (section 3.1). This serves to validate our numerical approach. We then consider the effects of radially dependent $\overline{\rho_c}(\bar{r})$ on the tunneling type electrical contacts (section 3.2). The one-dimensional MIM quantum tunneling equations [18, 19] are coupled with equations (4) and (5) and are solved self-consistently.

3. Results and discussion

3.1. Constant specific contact resistivity ρ_c along the radial contact length

For the special case of constant specific contact resistivity ρ_c, equation (4) can be rewritten as,

$$\frac{d^2\overline{V_g}(\bar{r})}{d\bar{r}^2} + \frac{1}{\bar{r}}\frac{d\overline{V_g}(\bar{r})}{d\bar{r}} - \left(1 + \overline{R_{sh2}}\right)\frac{\overline{V_g}(\bar{r})}{\overline{\rho_c}} = 0. \tag{6}$$

The corresponding boundary conditions from equations (5*a*) and (5*b*) are,

$$\overline{V_g}'(\bar{r} = 1) = \alpha,\ \overline{V_g}'(\bar{r} = \beta) = -\frac{\alpha\overline{R_{sh2}}}{\beta}. \tag{7}$$

Using equation (7), the solution to equation (6) is,

$$\overline{V_g}(\bar{r}) = aI_0(\lambda\bar{r}) + bK_0(\lambda\bar{r}), \quad \bar{r} > 0 \tag{8}$$

where I_0 and K_0 are the zeroth order modified Bessel functions of the first and second kind respectively and $\lambda = \sqrt{\left(1 + \overline{R_{sh2}}\right)/\overline{\rho_c}}$. The constants a and b are calculated from the boundary conditions as, $a = C/(CX + DY)$, $b = D/(CX + DY)$. The expressions of X, Y, C, and D are,

$$X = I_0(\lambda\beta) - \frac{I_0(\lambda\beta) - I_0(\lambda)}{\overline{\rho_c}\lambda^2} + \frac{\beta I_1(\lambda\beta)\ln\beta}{\overline{\rho_c}\lambda},$$

$$Y = K_0(\lambda\beta) - \frac{K_0(\lambda\beta) - K_0(\lambda)}{\overline{\rho_c}\lambda^2} - \frac{\beta K_1(\lambda\beta)\ln\beta}{\overline{\rho_c}\lambda},$$

$$C = \frac{\overline{R_{sh2}}K_1(\lambda) + \beta K_1(\lambda\beta)}{\lambda\beta[K_1(\lambda\beta)I_1(\lambda) - K_1(\lambda)I_1(\lambda\beta)]}, \text{ and}$$

$$D = \frac{\overline{R_{sh2}}I_1(\lambda) + \beta I_1(\lambda\beta)}{\lambda\beta[K_1(\lambda\beta)I_1(\lambda) - K_1(\lambda)I_1(\lambda\beta)]},$$

where I_1 and K_1 are the first order modified Bessel functions of the first and second kind respectively.

The normalized contact resistance is,

$$\overline{R_c} = \frac{\overline{V_1}(1) - \overline{V_2}(\beta)}{\alpha} = 1/\alpha = (CX + DY). \tag{9}$$

Figure 2 shows the profiles of voltage drop $\overline{V_g}(\bar{r})$ along the radial contact length $\bar{r}$ for a parallel annular thin film contact (figure 1) for different inner to outer radius ratio β (figure 2(a)), specific contact resistivity $\overline{\rho_c}$ (figure 2(b)), and sheet resistance ratio $\overline{R_{sh2}}$ (figure 2(c)). Note that, since $\overline{\rho_c}$ is constant along $\bar{r}$ here, the profiles of contact current density $\overline{J_c}(\bar{r}) = \overline{V_g}(\bar{r})/\overline{\rho_c}$ follow those of $\overline{V_g}(\bar{r})$. The voltage drop across the contact interface increases with increasing inner radius to outer radius ratio β and specific contact resistivity ρ_c. For similar contacting members ($\overline{R_{sh2}} = R_{sh2}/R_{sh1} = 1$) the maximum voltage drop occurs at the inner edge ($r = r_i$) of the annular contact (see figures 2(a) and (b)). This is because the modified Bessel function of the second kind (K_0 term in equation (8)) increases sharply near the center. Physically this means the current in the contact interface is mostly crowded near $r = r_i$. The current spreads out as it flows away from the center through the least resistive path. Figure 2(c) shows a similar trend in $\overline{V_g}(\bar{r})$ for dissimilar contacting members with $\overline{R_{sh2}} > 1$. In fact, the current crowding at the inner edge ($r = r_i$) increases with increasing $\overline{R_{sh2}}$. The voltage drop (and the contact current density) at the outer edge ($r = r_o$) increases with decreasing $\overline{R_{sh2}}$. For $\overline{R_{sh2}} \leqslant 0.1$, the majority of the contact current flows near $r = r_o$. It is interesting to note from figure 2(a) that the voltage drop profiles are highly asymmetric at the two edges ($r = r_i$, $r = r_o$) of the annular contact under study (figure 1) when β is small, and the asymmetry reduces as β increases. For the limiting case of $\beta \to 1$ (i.e. $r_i \approx r_o$), CTLM reduces to the planar limit [15], where the maximum voltage drop occurs at both the edges ($V_g(r = r_i) \approx V_g(r = r_o)$) and the minimum occurs at $(r_i + r_o)/2$, making the profiles symmetric.

The normalized contact resistance $\overline{R_c}$ is calculated from equation (9) and plotted in figures 3, 4, and 5 as functions of inner radius to outer radius ratio β, normalized specific contact resistivity $\overline{\rho_c}$, and sheet resistance ratio of the two contacting members $\overline{R_{sh2}}$, respectively. Figures 3(a) and (b) show that for $\beta < 0.8$, $\overline{R_c}$ decreases with β when $\overline{R_{sh2}}$ is high or $\overline{\rho_c}$ is low. Figures 4(b) and 5(b) also confirm this behavior. However, when β is increased above 0.8, R_c increases drastically with β. Larger β means shorter radial contact length $r_o - r_i$ (for a fixed r_i or r_o), resulting in higher total contact resistance for the annular contact structure. In general, $\overline{R_c}$ increases with the specific contact resistivity ρ_c or the sheet resistance ratio $\overline{R_{sh2}}$. Profiles of total contact resistance for the case of $\overline{R_{sh2}} = 0$ are also plotted in figures 3, 4 and 5 as dashed lines. When $\overline{R_{sh2}} \to 0$, equation (9) becomes,

$$\overline{R_c} = \frac{K_1(\lambda\beta)I_0(\lambda) + I_1(\lambda\beta)K_0(\lambda)}{\lambda[K_1(\lambda\beta)I_1(\lambda) - K_1(\lambda)I_1(\lambda\beta)]}, \tag{10}$$

with $\lambda = \sqrt{1/\overline{\rho_c}}$. Note that equation (10) is identical to the expression typically used for metal-semiconductor contact [9]. The difference between solid lines (equation (9)) and dashed lines (equation (10)) decreases when $\overline{\rho_c}$ or β is large, as shown in figures 3(b) and 4(b).

The dotted lines in figures 3(a), 4(b), and 5(b) are calculated from the contact resistance for parallel Cartesian contacts, that is, equation (8) of [15]. Note that the spatial dimensions were normalized by the contact length L ($= r_o - r_i$ in circular case) in [15], whereas they are normalized by the outer radius r_o for the circular case here. To make the normalization consistent for direct comparison, we multiply the normalized specific contact resistivity by $1/(1-\beta)^2$ before inserting into equation (8) of [15], which is multiplied by $(1-\beta)$ to obtain the dotted lines in figures 3(a), 4(b), and 5(b). For $\beta > 0.9$, the profiles of annular and Cartesian contact resistance match exceptionally well, as CTLM approaches the limit of Cartesian TLM.

3.2. *Tunneling dependent radially varying contact resistivity* ρ_c

Next, we consider the case where the parallel annular contacts are formed through a tunneling interface layer between the two annular contact members. In this case, due to the nonlinear current density–voltage ($J - V$) characteristic of metal-insulator-metal (MIM) tunnel junctions, specific contact resistivity ρ_c varies radially. For simplicity, we have made the following assumptions: (1) the thickness of the interfacial insulating film in the contact area is uniform and (2) the insulating film is sufficiently thin (in the nano- or subnano-meter scale) so that charge trappings are ignored [33, 34].

The local contact current density $J_c(r)$ at any location r from contact member 1 to contact member 2 is calculated based on the self-consistent 1D Schrödinger–Poisson solutions in the MIM junction [18, 19]. This quantum model includes emissions from both cathode (contacting member 2) and anode (contacting member 1), the effects of image charge potential [19], space charge, and exchange correlation potentials [35]. For given values of the work function of the two contact members $W_{1,2}$, electron affinity X, thickness D, and relative permittivity ε_r of the insulator layer, the local contact current density $J_c(r)$ can be calculated from this 1D quantum model for an input of the contact voltage drop $V_g(r)$ at any location r [18, 19]. The calculation of this $J_c(r)$- $V_g(r)$ relation is coupled with CTLM, equations (4), (5), and solved self-consistently.

We keep the same normalization as in section 2. Since solving the coupled quantum tunneling model [18, 19] and CTLM is time expensive, we calculate the one dimensional tunneling current density separately for the given MIM parameters (W_1, W_2, D, ε_r, X), over a wide range of bias voltages. The obtained $J-V$ curves are normalized (as in section 2) and then fitted with polynomials. Those curve-fitted equations are used to find the specific contact resistivity $\bar{\rho}_c(\bar{r}) = \overline{V_g}(\bar{r}) / \overline{J_c}(\bar{r}) = \left(\overline{V_1}(\bar{r}) - \overline{V_2}(\bar{r})\right) / \overline{J_c}(\bar{r})$, which is then inserted into the CTLM equations, equations (4) and (5), to give a self-consistent solution to the voltage and current profiles, as well as the contact resistance for the circular (annular) tunneling contact.

As an example, we consider Cu-vacuum-Cu circular thin film contacts. For our calculations, sub-nanometer scale interfacial layer thicknesses are assumed for the tunneling

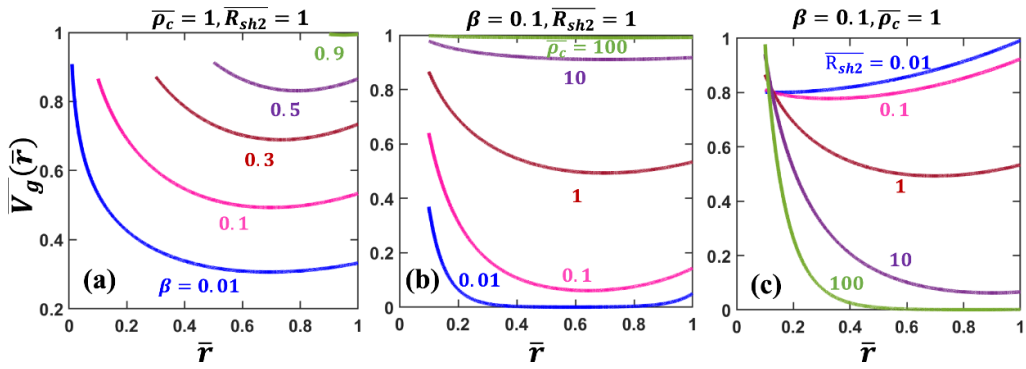

Figure 2. Normalized voltage drop across the contact interface $\overline{V_g}(\bar{r})$, along the radial direction of an annular contact with uniform contact resistivity, for different values of (a) inner radius to outer radius ratio β, with $\overline{\rho_c} = 1$ and $\overline{R_{sh2}} = R_{sh2}/R_{sh1} = 1$, (b) specific contact resistivity $\overline{\rho_c}$, with $\beta = 0.1$ and $\overline{R_{sh2}} = 1$, (c) sheet resistance ratio $\overline{R_{sh2}}$, with $\beta = 0.1$ and $\overline{\rho_c} = 1$. All the quantities are in their normalized forms defined in section 2.

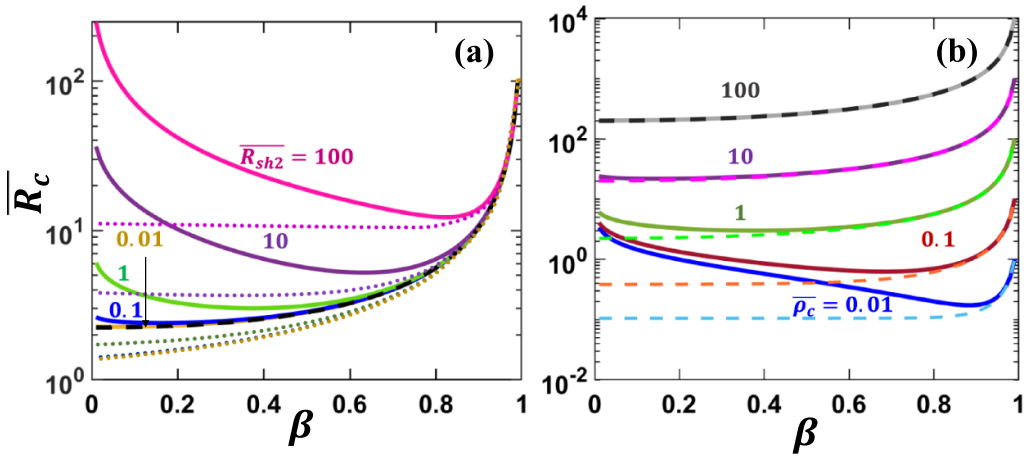

Figure 3. Normalized contact resistance $\overline{R_c}$ of the annular contact (figure 1) as a function of inner radius to outer radius ratio β for different (a) normalized sheet resistance of contacting member 2, $\overline{R_{sh2}}$, and (b) normalized specific contact resistivity $\overline{\rho_c}$. The dotted lines in (a) are calculated from equation (8) of [15], that is, for Cartesian parallel electrical contacts. Dashed lines are for equation (10), the limiting case of $\overline{R_{sh2}} \to 0$.

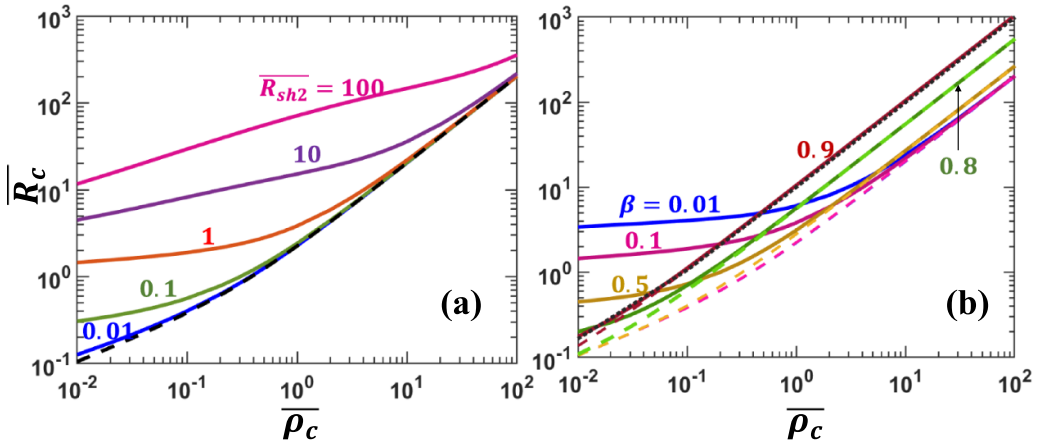

Figure 4. Normalized contact resistance $\overline{R_c}$ of the annular contact (figure 1) as a function of normalized specific contact resistivity $\overline{\rho_c}$ for different (a) normalized sheet resistance of contacting member 2, $\overline{R_{sh2}}$, and (b) inner radius to outer radius ratio β. In (a), $\beta = 0.1$, and in (b), $\overline{R_{sh2}} = 1$. Dashed lines are for equation (10), the limiting case of $\overline{R_{sh2}} \to 0$. The black dotted line in (b) is calculated from equation (8) of [15], that is, for Cartesian parallel electrical contacts.

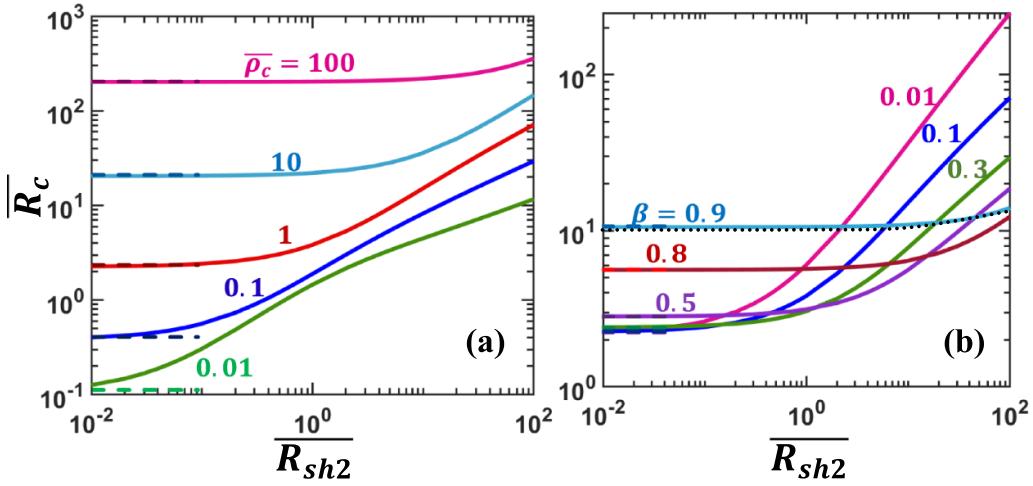

Figure 5. Normalized contact resistance $\overline{R_c}$ of the annular contact (figure 1) as a function of sheet resistance ratio $\overline{R_{sh2}}$ for different (a) normalized specific contact resistivity $\overline{\rho_c}$ and (b) inner radius to outer radius ratio β. In (a), $\beta = 0.1$, and in (b), $\overline{\rho_c} = 1$. Dashed lines are for equation (10), the limiting case of $\overline{R_{sh2}} \to 0$. The black dotted line in (b) is calculated from equation (8) of [15], that is, for Cartesian parallel electrical contacts.

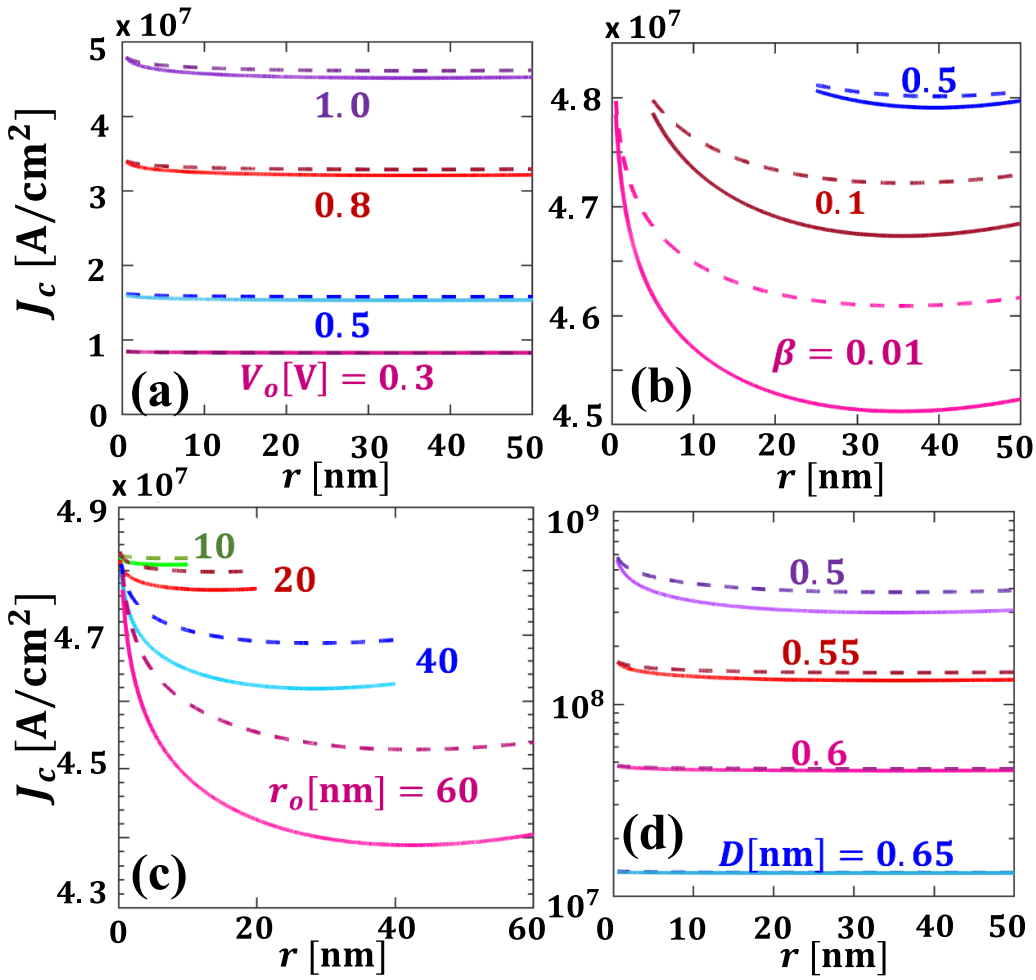

Figure 6. Tunneling current density across the contact interface $J_c(r)$ for different (a) input voltage V_0, with fixed $r_0 = 50$ nm, $\beta = 0.01$, and $D = 0.6$ nm; (b) inner radius to outer radius ratio β, with fixed $r_0 = 50$ nm, $V_0 = 1$ V, and $D = 0.6$ nm; (c) outer radius r_0, with fixed $V_0 = 1$ V, $\beta = 0.01$, and $D = 0.6$ nm; (d) interfacial layer thickness D, with fixed $r_0 = 50$ nm, $\beta = 0.01$, and $V_0 = 1$ V. All the material properties are specified in the main text. Solid lines are for self-consistent numerical calculations using equations (4) and (5), and MIM quantum tunneling formulations [18, 19]. Dashed lines are for analytical calculations from equation (8) with ρ_c being constant, calculated using $V_g = V_0$ in the MIM quantum model.

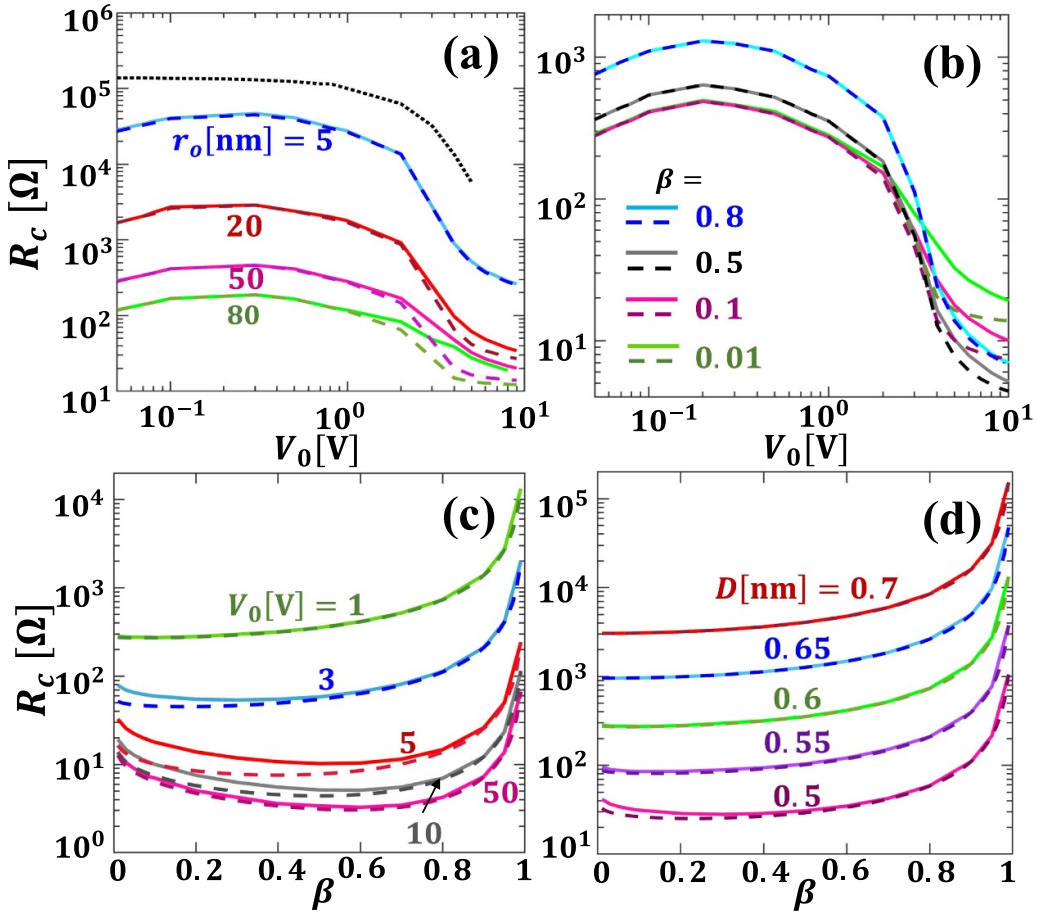

Figure 7. The total contact resistance R_c across the Cu-vacuum-Cu contact interface as functions of input voltage V_0 for different (a) outer radius r_0, with fixed $\beta = 0.01$ and $D = 0.6$ nm; (b) inner radius to outer radius ratio β, with fixed $r_0 = 50$ nm and $D = 0.6$ nm. R_c as functions of β for different (c) input voltage V_0, with fixed $r_0 = 50$ nm and $D = 0.6$ nm; (d) interfacial layer thickness D, with fixed $r_0 = 50$ nm and $V_0 = 1$ V. All of the material properties are specified in the main text. Solid lines are for self-consistent numerical calculations using equations (4) and (5), and MIM quantum tunneling formulations [18, 19]. The black dotted line in (a) is calculated using Simmons tunneling current formula [15, 27] and equations (4) and (5) for $r_o = 5$ nm. Dashed lines are for analytical calculations from equations (8) and (9) with ρ_c calculated using $V_g = V_0$ in the 1D MIM tunneling model.

type of electrical contacts [25, 36, 37]. The dimensions of the contacting members are assumed to be in nanoscale. We considered a wide range of electrode diameter, 10–160 nm, as electrodes of this range are common in transistors [38, 39], nanowire, nanofiber, and nanorod based novel devices [40–42]. Even though these nano structures are often referred to as one-dimensional because of their smaller diameters and longer lengths, our study shows that for precise characterization, two-dimensional analysis is necessary. In our calculation, sheet resistance of both the contact members is estimated as $R_{sh1} = R_{sh2} = 18\ \Omega/\square$ [43], where the unit of the sheet resistance $\Omega/\square$ means 'ohm per square' [8, 9, 44]. The work function of Cu thin films is $W_1 = W_2 =$ 4.56 eV [43]. The interfacial layer is assumed to be vacuum (relative permittivity $\varepsilon_r = 1.0$ and electron affinity $X = 0$ eV). The tunneling current density $J_c(r)$ through the contact interface is shown in figure 6 for various input voltages V_0 (figure 6(a)), inner radius to outer radius ratios β (figure 6(b)), outer radii r_0 (figure 6(c)), and interfacial layer thicknesses D (figure 6(d)). The profiles of $J_c(r)$ are asymmetric and current crowding occurs mainly at the inner edge, as expected for similar contact members (similar to figure 2 above). As shown in figure 6(a), because of the strong nonlinearity in the $J-V$ characteristics of a tunneling junction, $J_c(r)$ increases and exhibits a stronger radial dependence when the applied voltage V_o increases. This strong voltage dependence of electrical properties of the tunneling junction is in sharp contrast with those of ohmic contacts (section 3.1), where the profiles of $J_c(r)$ and the total contact resistance is independent of the applied voltage and the current density scales linearly with the voltage drop. Figure 6(b) shows that, as β decreases, that is, the contact length $r_o - r_i$ increases, the tunneling current density $J_c(r)$ decreases. The influence of outer radius r_o for a fixed β is shown in figure 6(c). The tunneling current density $J_c(r)$ decreases when r_o increases. However, the total current in the contact structure, $I_{tot} = \int_{r_i}^{r_o} 2\pi r\, J_c(r)\, dr$, increases with r_o because the total contact resistance of the tunneling junction decreases with r_o (see figure 7(a)). In figure 6(d), when the gap distance D increases, the current density $J_c(r)$ decreases quickly because the tunneling junction becomes more resistive [18, 19, 27].

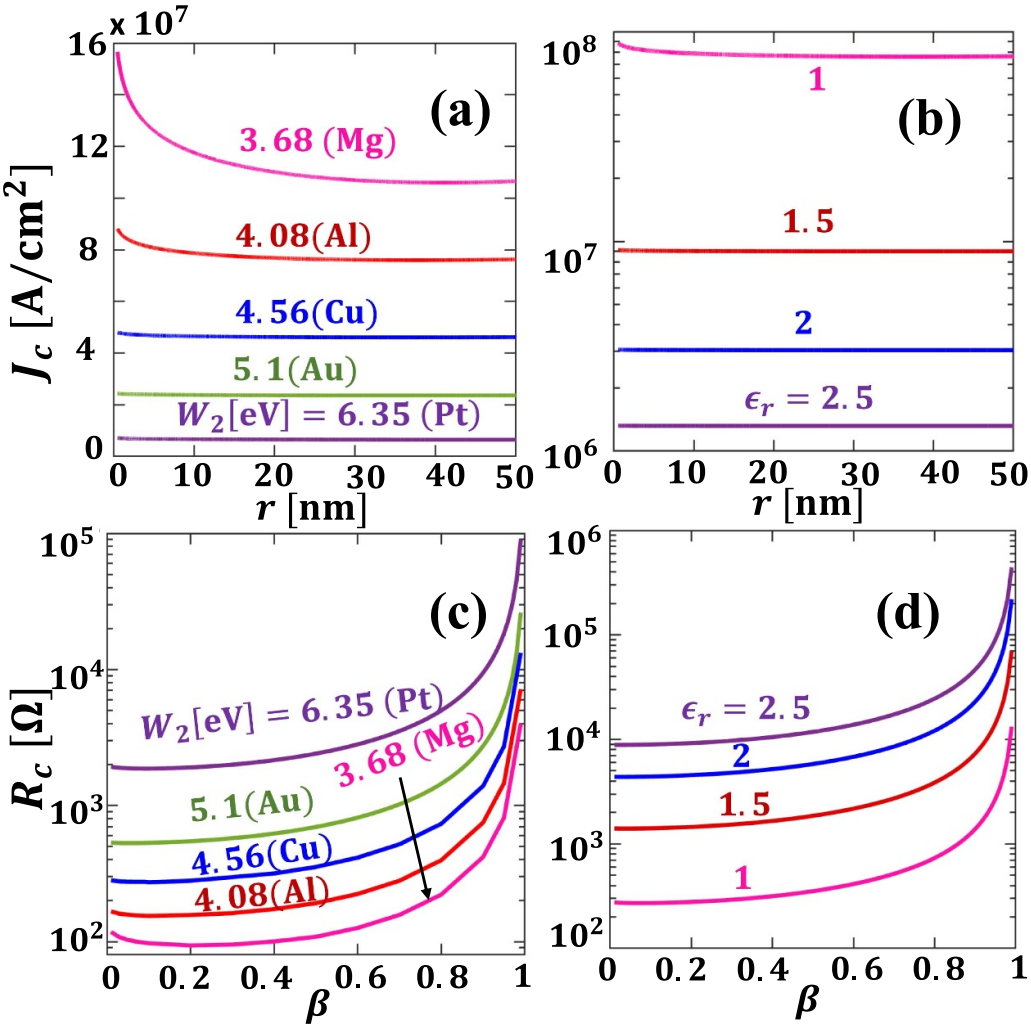

Figure 8. Tunneling current density across the Cu-insulator-metal contact interfaces $J_c(r)$ for different (a) contacting metals with work functions W_2 for fixed $\varepsilon_r = 1$, $r_0 = 50$ nm, $\beta = 0.01$, $D = 0.6$ nm, and $V_0 = 1$ V; (b) insulator layer permittivity ε_r for fixed $W_2 = 4.08$ eV (Al), $r_0 = 50$ nm, $\beta = 0.01$, $D = 0.6$ nm, and $V_0 = 1$ V. The total contact resistance R_c across the Cu-insulator-metal contact interfaces as functions of inner radius to outer radius ratio β for different: (c) W_2 for fixed $\varepsilon_r = 1$, $r_0 = 50$ nm, $D = 0.6$ nm, and $V_0 = 1$ V; (d) ε_r, for fixed $W_2 = 4.08$ eV (Al), $r_0 = 50$ nm, $D = 0.6$ nm, and $V_0 = 1$ V. All of the material properties are specified in the main text.

Dashed lines in figure 6 are the analytical results calculated from equation (8) assuming constant tunneling contact resistivity ρ_c across the radial contact length, which is the typically assumed one-dimensional tunneling contact. This ρ_c is calculated from the $J-V$ curve of the metal-insulator-metal tunneling junction by setting $V_g(r) = V_o$ everywhere along the contact length. The constant contact resistivity assumptions are inadequate, especially when the tunneling thickness D or inner radius to outer radius ratio β decreases, or the applied voltage V_o or outer radius r_o increases. For these cases, one should solve the coupled TLM equations, equations (4) and (5), and the localized MIM tunneling equation self-consistently to give more reliable predictions.

The total contact resistance R_c of the Cu-vacuum-Cu circular thin film contact is shown in figure 7 as functions of applied voltage V_0 and inner to outer radius ratio β. The total contact resistance R_c decreases with r_o, as shown in figure 7(a). As r_o increases, the dependence of contact resistance on r_o becomes less significant. The dashed lines are for analytical solutions of the 1D tunneling model with constant ρ_c calculated from equations (8) and (9) as previously stated. The difference between the 1D model (equation (9)) and self-consistent numerical calculations (equations (4) and (5)) is significant when D or β is small, or when r_o or V_0 is large. In these regimes where the 1D tunneling model with constant ρ_c approximations fail to provide reliable predictions, it is necessary to use the self-consistent numerical model.

The black dotted line in figure 7(a) is calculated using Simmons' tunneling current formula [15, 27] and equations (4) and (5) for $r_o = 5$ nm. Clearly, the difference between the quantum based self-consistent calculations and Simmons' formula is substantial. Simmons' formulas, which are widely used for these kinds of studies [15, 25], are inadequate in sub-nm scale (see figure 3(a) of [19]). For low applied voltages, in the direct tunneling regime, the MIM junction behaves ohmically, thus R_c varies slightly with V_0, as shown in figures 7(a) and (b). When the applied voltage is increased into the field

Table 1. Material parameters of the contacting metals in Cu-insulator-metal contacts.

Metal	W_2 (eV)	ρ_{bulk} (Ωm)	l (nm)
Mg	3.68 [52]	4.46×10^{-8} [53]	22.3 [50]
Al	4.08 [52]	2.65×10^{-8} [54]	18.9 [50]
Au	5.1 [19]	2.24×10^{-8} [53]	38 [47]
Pt	6.35 [52]	10.6×10^{-8} [54]	12 [51]

emission regime (>1 V), R_c decreases sharply with V_0. This is because the junction is no longer ohmic and the tunneling resistivity ρ_c decreases rapidly and nonlinearly with the junction voltage, which is a function of position along the radial contact length. As V_0 approaches 10 V, space charge effects become important [18, 19, 45, 46], and R_c saturates, decreasing only slightly with V_0.

The effect of the inner radius to outer radius ratio of the upper contact member (β) on the total contact resistance (R_c) is shown in figures 7(b)–(d), showing similar trends to figure 3(b) above for the case of constant contact resistivity ρ_c. Figure 7(d) shows that reducing the insulator layer thickness D even slightly can affect the contact resistance substantially.

Next, we extend our calculations for Cu thin film contacts to different metals: magnesium (Mg), aluminum (Al), gold (Au), and platinum (Pt). The resistivity of a metal thin film ρ_{film} is usually different than the metal's bulk resistivity ρ_{bulk}. ρ_{film} for the metals mentioned above are calculated from $\rho_{film}/\rho_{bulk} = 4/[3(t/l)\log(l/t)]$ for $t < l$ and $\rho_{film}/\rho_{bulk} = 1 + 3/8(l/t)$ for $t > l$ [47, 48], where l is the electron mean free path and t is the thickness of the thin film (figure 1). The work function [49], bulk resistivity ρ_{bulk}, and electron mean free path l [47, 50, 51] for the metals are given in table 1. The film thickness is assumed to be $t = 10$ nm for all the cases.

Figure 8 shows the effects of the work function of contacting member 2 (W_2) and the permittivity of the thin insulating layer (ε_r) on the electrical characteristics of Cu-insulator-metal contacts. Figure 8(a) shows that the tunneling current density $J_c(r)$ decreases with increasing W_2. Figure 8(b) shows that $J_c(r)$ reduces significantly when the permittivity of the insulating layer increases from 1 to 2.5. Figures 8(c) and (d) show the contact resistance (in Ω) for various contact metals and tunneling films for Cu-insulator-metal contacts as functions of β. Contact resistance increases with insulating layer permittivity ε_r and work function of contacting member 2, W_2. The potential barrier in the insulating layer increases with the increase of the work function of the contact metal, resulting in lower tunneling current and higher contact resistance. On the other hand, ε_r greatly influences the image charge potential and space charge potential [18, 19] in the contact interface.

4. Summary

In this paper, we present a self-consistent tunneling model to characterize parallel electrical contacts between two annular thin films. Our model considers the radial variation of contact resistivity along the contact length. We solved the CTLM equations for constant specific contact resistivity and radially varying, tunneling dependent specific contact resistivity along the contact length. Our study provides a thorough understanding of the contact tunneling resistance, current, and voltage distributions across nano and sub-nano scale MIM junctions in circular ring type electrical contacts using an inexpensive model from which many general scalings may be obtained. The effects of contact geometry (i.e. inner and outer radius of the ring contact, distance between the contact electrodes) and material properties (i.e. work function, sheet resistance of the contact members, and permittivity of the insulating layer) on the radial distributions of currents and voltages across these contacts and the overall contact resistance are studied in detail. The quantum tunneling model includes the effects of image charge, space charge, and exchange correlation potential.

It is found that the contact current density and voltage drop profiles are highly asymmetric at the two edges of the annular contact, even for similar contacting members. This is in sharp contrast to the current and voltage profiles of parallel Cartesian nanocontacts. However, the asymmetry reduces when inner radius to outer radius ratio β increases; for $\beta \to 1$, the profiles become almost symmetric. Our calculations for tunneling type contacts show that the contact resistance R_c is voltage dependent, increases sharply with D, and decreases with r_o. If β is increased above 0.9, the R_c of the annular contact increases dramatically. It is found that the analytical solutions of one-dimensional (1D) tunneling junction models (constant voltage across the whole junction) are good approximations of the actual circular (annular) contacts only when the thickness D or inner radius to outer radius ratio β is relatively large, or the applied voltage across the contact V_0 or outer radius r_o is relatively small. Otherwise, the 1D tunneling model of constant contact resistivity becomes unreliable, and the self-consistent CTLM equations coupled with the spatially dependent tunneling current need to be used to accurately characterize the electrical contacts.

In existing CTLM [11, 12], the interface contact resistivity is almost always assumed to be constant. Thus, the contact resistivity measured using the transmission line method (TLM) would consist of possible intrinsic errors when a thin tunneling (e.g. oxide) layer at the contact interfaces is present. In this case, our model would give a more accurate evaluation of contact resistivity. The work presented here may be used to better understand the electrical conductivity of nanofiber and nanorod contacted thin-film devices, where such circular (or annular) contacts naturally exist. Furthermore, our study reveals that, by varying the contact layer properties and geometry, one can strategically design the radially dependent contact resistivity in circular contacts to achieve desired current distribution. It is worth mentioning that while the work presented here is for tunneling type contacts, our modified CTLM equations with radially varying ρ_c can also be used for other types of contacts such as ohmic and Schottky contacts.

Although a TLM is less computationally expensive and easier to implement, it is a simplified approximation of practical 2D electrical contacts. Field solution methods need to be used in the future to accurately evaluate current crowding and fringing field effects, the impact of finite thickness (or length)

in the contact members, and the possible parallel component of current flows in the interface layer [8, 15, 44, 55, 56]. The effects of reactive elements in the circuit, AC response, and imperfect insulator layer on the electrical properties of tunneling type contacts may also be studied in the future. Future studies may also consider the influence of properties of the materials forming the contact and the possible interaction of the semiconductor (or insulator) films under the contact region, such as Schottky barrier, band bending, charge redistribution, and material defects.

Acknowledgments

The work is supported by the Air Force Office of Scientific Research (AFOSR) YIP Award No. FA9550-18-1-0061.

ORCID iD

Peng Zhang https://orcid.org/0000-0003-0606-6855

References

[1] Frank D J, Dennard R H, Nowak E, Solomon P M and Taur Y 2001 Device scaling limits of Si MOSFETs and their application dependencies *Proc. IEEE* **89** 259–88
[2] Franklin A D, Farmer D B and Haensch W 2014 Defining and overcoming the contact resistance challenge in scaled carbon nanotube transistors *ACS Nano* **8** 7333–9
[3] Vazirisereshk M R, Sumaiya S A, Martini A and Baykara M Z 2019 Measurement of electrical contact resistance at nanoscale gold-graphite interfaces *Appl. Phys. Lett.* **115** 091602
[4] Houssa M *et al* 2019 Contact resistance at MoS_2-based 2D metal/semiconductor lateral heterojunctions *ACS Appl. Nano Mater.* **2** 760–6
[5] Tang J *et al* 2018 Flexible CMOS integrated circuits based on carbon nanotubes with sub-10 ns stage delays *Nat. Electron.* **1** 191–6
[6] Peng L-M 2018 A new stage for flexible nanotube devices *Nat. Electron.* **1** 158–9
[7] Allain A, Kang J, Banerjee K and Kis A 2015 Electrical contacts to two-dimensional semiconductors *Nat. Mater.* **14** 1195–205
[8] Zhang P and Lau Y Y 2014 An exact field solution of contact resistance and comparison with the transmission line model *Appl. Phys. Lett.* **104** 204102
[9] Schroder D K 1998 *Semiconductor Material and Device Characterization* 2nd edn (New York: Wiley)
[10] Zhang P, Valfells Á, Ang L K, Luginsland J W and Lau Y Y 2017 100 years of the physics of diodes *Appl. Phys. Rev.* **4** 011304
[11] Reeves G K 1980 Specific contact resistance using a circular transmission line model *Solid State Electron.* **23** 487–90
[12] Xu C, Wang J, Wang M, Jin H, Hao Y and Wen C P 2006 Reeves's circular transmission line model and its scope of application to extract specific contact resistance *Solid State Electron.* **50** 843–7
[13] Patel K N, Stokes E, Pagan J, Burkhart C C, Hodge M and Batoni P 2007 Circular transmission line model (CTLM) analysis for non-linear VI characteristics on Mg doped GaN *ECS Trans.* **11** 203–8
[14] Murrmann H and Widmann D 1969 Current crowding on metal contacts to planar devices *IEEE Trans. Electron Devices* **16** 1022–4
[15] Banerjee S, Luginsland J and Zhang P 2019 A two dimensional tunneling resistance transmission line model for nanoscale parallel electrical contacts *Sci. Rep.* **9** 1–14
[16] Zhang P, Fairchild S B, Back T C and Luo Y 2017 Field emission from carbon nanotube fibers in varying anode-cathode gap with the consideration of contact resistance *AIP Adv.* **7** 125203
[17] Fairchild S B *et al* 2019 Carbon nanotube fiber field emission array cathodes *IEEE Trans. Plasma Sci.* **47** 2032–8
[18] Banerjee S and Zhang P 2019 A generalized self-consistent model for quantum tunneling current in dissimilar metal-insulator-metal junction *AIP Adv.* **9** 085302
[19] Zhang P 2015 Scaling for quantum tunneling current in nano- and subnano-scale plasmonic junctions *Sci. Rep.* **5** 9826
[20] Banerjee S, Cao L, Ang Y S, Ang L K and Zhang P 2020 Reducing contact resistance by roughness engineering in 2D-material-based electrical contacts *Phys. Rev. Appl.* accepted
[21] de Lima J A, Gimenez S P and Cirne K H 2012 Modeling and characterization of overlapping circular-gate MOSFET and its application to power devices *IEEE Trans. Power Electron.* **27** 1622–31
[22] Trudeau P-E, Sheldon M, Altoe V and Alivisatos A P 2008 Electrical contacts to individual colloidal semiconductor nanorods *Nano Lett.* **8** 1936–9
[23] Cronin S B *et al* 2002 Making electrical contacts to nanowires with a thick oxide coating *Nanotechnology* **13** 653–8
[24] Khan K *et al* 2020 Recent developments in emerging two-dimensional materials and their applications *J. Mater. Chem.* C **8** 387–440
[25] Li C, Thostenson E T and Chou T-W 2007 Dominant role of tunneling resistance in the electrical conductivity of carbon nanotube–based composites *Appl. Phys. Lett.* **91** 223114
[26] Lord A M *et al* 2015 Controlling the electrical transport properties of nanocontacts to nanowires *Nano Lett.* **15** 4248–54
[27] Simmons J G 1963 Generalized formula for the electric tunnel effect between similar electrodes separated by a thin insulating film *J. Appl. Phys.* **34** 1793–803
[28] Simmons J G 1963 Electric tunnel effect between dissimilar electrodes separated by a thin insulating film *J. Appl. Phys.* **34** 2581–90
[29] Pop E 2010 Energy dissipation and transport in nanoscale devices *Nano Res* **3** 147–69
[30] Hu X and Martini A 2017 Atomistic simulations of contact area and conductance at nanoscale interfaces *Nanoscale* **9** 16852–7
[31] Berger H H 1972 Contact resistance and contact resistivity *J. Electrochem. Soc.* **119** 507–14
[32] Simmons J G 1971 Conduction in thin dielectric films *J. Phys. D: Appl. Phys.* **4** 613–57
[33] Rose A 1955 Space-charge-limited currents in solids *Phys. Rev.* **97** 1538–44
[34] Frank R I and Simmons J G 1967 Space-charge effects on emission-limited current flow in insulators *J. Appl. Phys.* **38** 832–40
[35] Perdew J P and Wang Y 1992 Accurate and simple analytic representation of the electron-gas correlation energy *Phys. Rev.* B **45** 13244–9
[36] Tsagarakis M S and Xanthakis J P 2017 Tunneling currents between carbon nanotubes inside the 3-dimensional potential of a dielectric matrix *AIP Adv.* **7** 075012
[37] Wu L, Duan H, Bai P, Bosman M, Yang J K W and Li E 2013 Fowler-Nordheim tunneling induced charge transfer plasmons between nearly touching nanoparticles *ACS Nano* **7** 707–16

[38] Ieong M, Doris B, Kedzierski J, Rim K and Yang M 2004 Silicon device scaling to the sub-10-nm regime *Science* **306** 2057–60
[39] Zheng J *et al* 2013 Sub-10 nm gate length graphene transistors: operating at terahertz frequencies with current saturation *Sci. Rep.* **3** 1–9
[40] Ghamsari M S and Dhara S 2020 *Nanorods and Nanocomposites* (Rijeka: InTechOpen)
[41] Mackey M A, Ali M R K, Austin L A, Near R D and El-Sayed M A 2014 The most effective gold nanorod size for plasmonic photothermal therapy: theory and *in vitro* experiments *J. Phys. Chem.* B **118** 1319–26
[42] Wawra S E, Pflug L, Thajudeen T, Kryschi C, Stingl M and Peukert W 2018 Determination of the two-dimensional distributions of gold nanorods by multiwavelength analytical ultracentrifugation *Nat. Commun.* **9** 1–11
[43] Schmiedl E, Wissmann P and Finzel H-U 2014 The electrical resistivity of ultra-thin copper films *Z. Naturforsch.* A **63** 739–44
[44] Zhang P, Lau Y Y and Gilgenbach R M 2015 Analysis of current crowding in thin film contacts from exact field solution *J. Phys. D: Appl. Phys.* **48** 475501
[45] Lau Y Y, Chernin D, Colombant D G and Ho P-T 1991 Quantum extension of Child-Langmuir law *Phys. Rev. Lett.* **66** 1446–9
[46] Ang L K, Kwan T J T and Lau Y Y 2003 New scaling of Child-Langmuir law in the quantum regime *Phys. Rev. Lett.* **91** 208303
[47] Chopra K L, Bobb L C and Francombe M H 1963 Electrical resistivity of thin single-crystal gold films *J. Appl. Phys.* **34** 1699–702
[48] Fuchs K 1938 The conductivity of thin metallic films according to the electron theory of metals *Math. Proc. Camb. Phil. Soc* **34** 100–8
[49] Lide D R, Baysinger G, Chemistry S, Berger L I, Goldberg R N and Kehiaian H V 2003 *CRC Handbook of Chemistry and Physics* (Boca Raton, FL: CRC Press)
[50] Gall D 2016 Electron mean free path in elemental metals *J. Appl. Phys.* **119** 085101
[51] Fischer G, Hoffmann H and Vancea J 1980 Mean free path and density of conductance electrons in platinum determined by the size effect in extremely thin films *Phys. Rev.* B **22** 6065–73
[52] Tipler P A and Llewellyn R 2012 *Modern Physics* 6th edn (San Francisco, CA: Freeman)
[53] Engineering Toolbox 2003 Resistivity and conductivity-temperature coefficients for common materials (https://www.engineeringtoolbox.com/resistivity-conductivity-d_418.html)
[54] Giancoli D C 1995 *Physics* 4th edn (Englewood Cliffs, NJ: Prentice Hall)
[55] Zhang P, Hung D M H and Lau Y Y 2013 Current flow in a 3-terminal thin film contact with dissimilar materials and general geometric aspect ratios *J. Phys. D: Appl. Phys.* **46** 065502
[56] Zhang P, Lau Y Y and Gilgenbach R M 2010 Minimization of thin film contact resistance *Appl. Phys. Lett.* **97** 204103